Confinement-Induced vs. Correlation-Induced Electron Localization in Model Semiconductor Nano Circuits

A. Franceschetti [(1)], L.W. Wang [(2)], G. Bester [(1)], and A. Zunger [(1)]

(1) National Renewable Energy Laboratory, Golden, CO 80401

(2) Computational Research Division, Lawrence Berkeley National Laboratory, Berkeley, CA 94720

Abstract

Single-particle plus many-particle calculations of the electronic states of semiconductor nano dumbbells illustrate how geometrical features (e.g. the width of the dumbbell wire) determine, through quantum confinement and electron-electron correlation effects, the localization of the wave functions. Remarkably, we find that many-body effects can alter carrier localization, thus affecting the transport properties of nano circuits that include quantum dots and quantum wires. This is important, as most of the current transport calculations (using Landauer formula) neglect many-particle effects. We further show how the degree of entanglement and the exciton binding energies depend on the nano circuit geometry.

The current technological pursuit of electronic nano devices [1-6], based on 2D quantum wells, 1D quantum wires, and 0D quantum dots of ever decreasing sizes, is rapidly approaching systems where carrier localization and transport are entirely controlled by quantum effects. Transistors made of a carbon nanotube [1], or a single semiconductor nanowire [2], or a few colloidal nanocrystals [3], as well as single electron [4,5] or hole [6] tunneling into gated quantum dots, all exemplify the trend towards low-dimensionality and nanometer-sized circuit components, as envisioned by the electronic industry roadmap [7]. Most theoretical descriptions of nano systems pertain to isolated *building blocks* of nano-circuits, such as 0D quantum dots [8], 1D quantum wires [9], and 2D quantum wells [10], and little is known on the quantum behavior of complex *assemblies* of such building blocks. Recent calculations on simple assemblies of nanostructures of the *same dimensionality*, such as 0D diatomic "dot molecules" [11] or 0D "dot crystals" [12], have already revealed the importance of potentially transport-impeding effects, such as correlation-induced (Mott) localization of the carriers on fragments (building blocks) of the entire system. Despite this intiuitive knowledge, most transport calculations in molecules and nanostructures use the Landauer formula [13], which neglects many-body effects. Of particular interest here are such quantum effects in *mixed-dimensionality* systems (e.g. dots + wires), which are the necessary architectural elements of nano circuits [7]. Consider, for example, the simplest combination of building blocks of different dimensionalities: A "nano dumbbell" made of two 0D dots of radius R_D connected by a 1D wire of radius R_W. Such systems have been recently made, e.g. by Mokari et al. [14]. Figure 1 illustrates how the *single-particle* electronic structure

could depend critically on the wire radius R_W. For a *wide* wire (Fig. 1a), reduced quantum confinement in the wire causes the wire electron energy level e_W to drop *below* the dot energy levels e_D, with ensuing localization of the electron wavefunction on the 1D *wire* segment. For a *narrow* wire (Fig. 1b), increased quantum confinement in the wire raises the energy level e_W *above* e_D, leading to migration of the wave function into the 0D *dots*. It is likely, however, that many-particle effects could modify this picture in a substantial way. Consider, for example, the case of two electrons simultaneously present in the dumbbell system. Electron correlation induced by the energetic and spatial proximity of various single-particle levels of Fig. 1 would lead to a *mixture* of the single-particle ground and excited states. Depending on the relative sizes R_D and R_W, the many-particle wave function (made of a coherent superposition of single-particle states) could be delocalized over the entire wire+dots system, even though the lowest-energy single-particle state is localized only on the wire. Clearly, a proper theory of carrier localization and transport in nanocircuits must include both single-particle and many-particle effects [15].

Several methodologies are available in the literature for combining a single-particle description with a many-body treatment. "First-generation" approaches are based on (i) *continuum* effective-mass single-particle theories, such as the one-band particle-in-a-box effective-mass approximation (see e.g. Ref. [16]) or the few-band **k.p** approximation (e.g. Ref. [17]). These single-particle approaches model quantum confinement, but either neglect [16] or oversimplify [17] the effects of inter-band coupling (e.g. the coupling between various bands at a given point of the Brillouin zone), inter-valley coupling (e.g. between the Γ, X, and L valleys), as well as surface effects [17] and strain effects [16].

These approximations lead to quantitative errors [18], and often even to a qualitative misrepresentation of the correct nanostructure symmetry (the so called "farsightedness effect" [19]). These continuum-like effective-mass approaches have been combined with many-body treatments such as quantum Monte Carlo [20] or configuration interaction (either for **k.p** [21] or for the single-band effective mass [22]), enabling calculations of large (up to 10^7 atom) systems. "Second generation" approaches are based on (ii) *atomistic* single-particle theories (such as tight-binding [23] or empirical pseudopotentials [24]) which include a broad range of single-particle effects (e.g. inter-band and inter-valley coupling, surface passivation, strain, compositional inhomogeneity), albeit via empirical parametrization of the *bulk* Hamiltonian. These approaches have also been combined with many-body approaches, such as configuration-interaction (either in the context of tight-binding [25] or pseudopotentials [26]), enabling calculations on 10^3-10^6 atom systems [11,26]. What we are aiming at is a "third-generation" approach, based on (iii) *first*-principles atomistic single-particle theories (such as plane-wave LDA) combined with a sophisticated many-body approach. To date, such combinations of methodologies are limited to tiny nanostructures [27, 28], because both the single-particle LDA method and the many-body approaches are enormously demanding from a computational point of view. Here we combine an atomistic, LDA-quality single-particle "charge-patching" approach [29] with a configuration-interaction many-particle method [26] to calculate quantum confinement and electron localization in semiconductor nano dumbbells containing up to 6,000 atoms. We show how single-particle effects lead to specific localization patterns, and how many-body effects can reverse them. The significance of such calculations is in elucidating the way that the

geometry and dimensionality of the building blocks of a model nano circuit can affect carrier localization and transport through a conspiracy of single-particle and many-particle effects.

We consider here nano dumbbells consisting of two nearly-spherical CdTe dots (R_D = 25 Å) connected by a 30 Å-long CdSe wire of variable radius R_W. Both the dots and the wire have the zinc-blende lattice structure with the axis of the wire in the (001) direction. Surface atoms are passivated using a ligand-like potential. Figure 2 shows the atomistic structure of one of the nano-dumbbells used in the calculations. This system consists of nnn Cd, Se, and Te atoms plus nnn passivants. The atomic positions are relaxed using an atomistic valence force field model. The total valence charge density of the relaxed system is constructed using the charge-patching method [29]. In this method, small prototype systems with similar local atomic structures as the dumbbell are calculated selfconsistently with density functional theory (DFT). The total valence charge densities of these prototype systems are decomposed into charge motifs belonging to different atoms. Then these charge motifs are assembled together to generate the charge density of the dumbbell. The typical density error generated this way is less than 1% compared with direct ab initio selfonsistent calculations. The resulting absolute eigen energy error is about 20 meV, and inter state splitting energy error is less than a few meV. After the charge density is obtained, the local density approximation formula of DFT is used to generate the total potential, and the single particle Schrodinger's equation is solved using the folded spectrum method [24]. The detail procedure of the charge patching method was reported in Ref.[30].

The calculated *single-particle* wave functions and energies of several near-edge states are shown in Fig. 3 for three values of R_W. The localization of near-edge states can be understood qualitatively by considering the CdSe wire and the two CdTe dots as separate building blocks, and allowing perturbative coupling between wire (W) and dots (D_1 and D_2) single-particle states, as illustrated in Fig. 4. For all the dumbbell geometries considered here, the valence-band maximum (VBM) is an anti-bonding combination of the two s-like valence states localized on the CdTe dots (bottom panels of Fig. 3). This is so because the valence band offset between CdTe and CdSe [31] (see Fig. 1) places the VBM of CdSe deeper in energy. Figure 3 shows that the wave function character of the conduction-band minimum (CBM) depends strongly on the radius R_W of the wire. In the case of a narrow wire (Figs. 3a and 4a), quantum-confinement pushes the energy of the wire states well *above* the lowest-energy dot states, and coupling between dot states and wire states is relatively small. As a result, the lowest-energy electron states, ψ_1 and ψ_2, correspond to bonding and anti-bonding combinations of pure dot states ($D_1 \pm D_2$), as shown in Figs. 3a and 4a. In the opposite case of a wide wire (Figs. 3c and 4c), the lowest-energy wire state (W) drops *below* the dot states ($D_1 \pm D_2$) as a result of reduced quantum confinement. The CBM ψ_1 corresponds to an s-like state localized on the wire (Figs. 3c and 4c). The next two states ψ_2 and ψ_3 are also localized on the wire, and have p_x-like and p_y-like envelope functions, respectively. In the case of a wire of intermediate size (Figs. 3b and 4b), we observe strong coupling between wire and dots conduction states. The dot-dot bonding state (D_1+D_2) is strongly coupled to the wire s-like state (W). This coupling leads to a CBM made of the bonding combination $\psi_1 = D_1+D_2+W$. Interestingly, the anti-bonding combination $\psi_3 = D_1+D_2-W$ is higher in energy than the

dot-dot anti-bonding state $\psi_2=D_1-D_2$, because by symmetry D_1-D_2 cannot couple to wire s-like states.

To examine the effects of electron-electron interactions on the localization of the wave functions, we consider a system of two conduction-band electrons in the dumbbell. The calculation of the many-body states is performed using the configuration-interaction (CI) approach described in Ref. [26]. First, we calculate screened electron-electron Coulomb and exchange integrals of the form:

$$J_{ij,kl} = \sum_{\sigma\sigma} \int\int \psi_i^*(\boldsymbol{r},\sigma)\psi_j^*(\boldsymbol{r}',\sigma') \frac{e^2}{\bar{\varepsilon}(\boldsymbol{r},\boldsymbol{r}')\,|\,\boldsymbol{r}-\boldsymbol{r}'|} \psi_k(\boldsymbol{r},\sigma)\psi_l(\boldsymbol{r}',\sigma') d\boldsymbol{r} d\boldsymbol{r}',$$

where $\psi_i(\boldsymbol{r},\sigma)$ are the single-particle wave functions (Fig. 3), which depend on the spatial variable $\boldsymbol{r}$ and the spin variable σ. The Coulomb interaction is screened by the dielectric function, which we assume [32] to have the bulk value of the constituents inside the dumbbell, and to decay to $\varepsilon_{out}=1$ outside. Next, we set up and diagonalize the configuration-interaction Hamiltonian using a basis set of Slater determinants (configurations). In all cases considered here, the basis set consists of the orbital and spin configurations constructed from the first three conduction-band states (ψ_1, ψ_2, and ψ_3), corresponding to a total of 15 Slater determinants. All other conduction-band states are much higher in energy, so their contribution to low-energy many-particle states is small. Once the many-particle wave functions have been obtained, we calculate the degree of entanglement (DOE) using a generalization of the Von Neumann definition of entanglement to identical fermions [33]. We also calculate the pair correlation function **(GB: show formula here)**, which gives the probability to find and electron at $\boldsymbol{r}$ given that the second electron is located at $\boldsymbol{r}$' [33].

The results of the many-body calculations are shown in Figs. 5-7, where, for transparency of the pertinent physics, we consider four levels of approximation (from left to right in each figure): (a) In the single-particle approximation, the energy of the configuration $|\psi_i\ \psi_j>$ (a single Slater determinant constructed from the single-particle orbitals ψ_i and ψ_j) is given by the sum of the single-particle energies ($\varepsilon_i + \varepsilon_j$). (b) In the next level of approximation (single-particle plus diagonal Coulomb), we include the diagonal Coulomb energies ($J_{ij,ij}$), describing the direct repulsion between an electron in the single-particle state ψ_i and an electron in ψ_j. This is equivalent to first-order perturbation theory [14]. (c) In the "single-configuration" approximation, the Coulomb and exchange interactions between different spin configurations corresponding to the same orbital configuration are included. Thus, each configuration $|\psi_i\ \psi_j>$ (with $i \neq j$) splits into a singlet and a triplet. (d) Finally, in the full configuration-interaction calculations all the orbital and spin configurations consistent with a given number of single-particle states are used to expand the many-body wave functions.

In the case of the wide-wire dumbbell the first few conduction states (ψ_1, ψ_2, and ψ_3) are all localized on the wire, and are separated by large energy spacings (Fig. 3c). As a result, correlation effects are small (Fig. 5), and the two electrons in the dumbbell form a singlet state $|\psi_1\psi_1>$ corresponding to double occupancy of the lowest-energy wire state ψ_1. Since the ground state can be described by a single Slater determinant, the DOE is nearly zero. The correlation function (bottom panel of Fig. 5) is very similar in the correlated and uncorrelated cases. If one electron (blue circle) is placed at the center of the wire, then the second electron (orange cloud) is also localized on the wire. The

excited states are a singlet and a triplet derived from $|\psi_1\psi_2>$, with an exchange splitting of 64 meV.

In the opposite situation of a thin-wire dumbbell (Fig. 6), the first two conduction states (ψ_1 and ψ_2) are bonding and anti-bonding linear combinations of dots states, respectively (Fig. 3a). We can construct three configurations of the two-electron system using ψ_1 and ψ_2: two singly-degenerate configurations $|\psi_1\psi_1>$ and $|\psi_2\psi_2>$, and one four-fold degenerate configuration $|\psi_1\psi_2>$. These configurations are shifted up in energy by direct electron-electron Coulomb interaction (Fig. 6b). The electron-electron exchange interaction (Fig. 6c) splits the configuration $|\psi_1\psi_2>$ into a singlet and a triplet, separated by 110 meV. Finally, configuration interaction strongly (Fig. 6d) mixes the configurations $|\psi_1\psi_1>$ and $|\psi_2\psi_2>$, leading to a many-body singlet ground-state that is a linear combination of those two configurations. This state has the maximum degree of entanglement (DOE=100%). Since in the single-particle description the first wire state is significantly higher in energy than the dot states (Fig. 3a), the physics of the two-electron dumbbell system is analogous to that of two dots without a connecting wire [33]: The first four states correspond to the two electrons being localized on different dots (with the singlet state slightly lower in energy than the triplet state), as a result of electron-electron repulsion. The next two states correspond to the two electrons being localized on the same dot. The localization of the electrons on opposite dots is driven by correlation effects, as demonstrated by the correlation function plot shown at the bottom of Fig. 6: When one electron is located at the center of the left dot (blue dot), then the second electron (yellow cloud) is delocalized on both dots in the uncorrelated case, but only on the right-hand side dot in the correlated case.

Finally, we consider the case of intermediate wire thickness (Fig. 7). In this case there are several configurations in a narrow (<100 meV) energy interval. An immediate consequence is that direct Coulomb interactions change the order of the configuration energies. Configurations that are four-fold degenerate (due to spin degeneracy) at the single-particle level (Fig. 7a and 7b), split in the single-configuration approximation (Fig. 7c) into a singlet and a triplet. The ground state is the triplet state originating from the configuration $|\psi_1\psi_2>$. However, configuration interaction mixes states of the same spin multiplicity, leading to a ground state that has contributions from several configurations ($|\psi_1\psi_1>$, $|\psi_1\psi_3>$, and $|\psi_2\psi_2>$), as shown in Fig. 7d. Strong correlation effects alter the distribution of the two electrons: A plot of the correlation function (bottom of Fig. 7) shows that while the two electrons are localized mainly on the wire in the uncorrelated case, they are located on the dots when configuration interaction is taken into account. The degree of entanglement in this case takes an intermediate value of 61%, showing a certain mixing of configurations that does not lead, however, to a purely symmetric or antisymmetric state with maximum entanglement. The next excited states originate from the $|\psi_1\psi_2>$ triplet states with some admixture of $|\psi_2\psi_3>$ character. These 3 fold degenerate states have a degree of entanglement between 80 and 97%.

The localization of the single-particle wave functions has direct consequences on the optical properties of the nano dumbbells. As the wire becomes narrower, the CBM wave function migrates from the CdSe wire to the CdTe dots, while the VBM wave function remains localized on the CdTe dots, as shown in Fig. 3. Thus, the band alignment of the dumbbell changes from type-I to type-II, affecting the exciton binding energy. We have calculated the exciton energies of the nano dumbbells using the configuration-interaction

approach [26]. We have included two valence-band states and two conduction-band states in the CI expansion. The exciton binding energy is given by $E_b = E_X^0 - E_X$, where E_X^0 is the energy of the lowest electron-hole pair in the un-correlated (single-particle) case, and E_X is the energy of the exciton in the CI calculation. For a narrow CdSe wire (R_w = 8Å) both the VBM and the CBM wave functions are localized on the CdTe dots, resulting in a relatively large electron-hole binding energy (E_b=115 meV). As the CdSe wire becomes wider, the exciton binding energy decreases to 86 meV for R_w = 10 Å and 59 meV for R_w=15 Å.

In conclusion, we have shown that the localization of single-particle wavefunctions in CdSe/CdTe nano dumbbells can be controlled by changing the radius of the CdSe wire. As the wire becomes narrower, the wire electron states are pushed higher in energy compared to the dot electron states, so the lowest electron state changes its localization from the wire to the dots. When the band-edge states of the CdSe wire are brought into resonance with those of the CdTe dots, strong correlation effects dominate the spatial localization and the degree of entanglement of the two-electron wave functions. These results illustrate how quantum confinement and correlation effects determine carrier localization and electronic transport in semiconductor nano devices. [possible sentences to add]: Our work demonstrated that composite nanostructures like the dumbbell can serve as platforms to manipulate the many-body effects and quantum entanglements, thus they can be used for studying the basic quantum physics, and at the same time for potential quantum electronic device and quantum computing applications.

This work was supported by the DOE-SC-BES initiative LAB03-17, under NREL Contract No. DE-AC36-99GO10337, and LBNL Contract No. DE-AC03-76SF00098.

This research used the resources of the National Energy Research Scientific Computing Center.

References

[1] P.G. Collins and P. Avouris, *Scientific American* **283**, 62 (2000).

[2] Y. Huang, X. Duan, Y. Cui, L.J. Lauhon, K.H. Kim, and C.M. Lieber, *Science* **294**, 1313 (2001).

[3] D.L. Klein, R. Roth, A.K.L. Lim, A.P. Alivisatos, and P.L. McEuen, *Nature* **389**, 699 (1997).

[4] S. Tarucha, D.G. Austing, T. Honda, R.J. van der Hage, and L.P. Kouwenhoven, *Phys. Rev. Lett.* **77**, 3613 (1996); L.P. Kouwenhoven, T.H. Oosterkamp, M.W.S. Danoesastro, M. Eto, D.G. Austing, T. Honda, and S. Tarucha, *Science* **278**, 1788 (1997)

[5] R.J. Warburton, C Schaflein, D. Haft, F. Bickel, A. Lorke, K. Karrai, J.M. Garcia, W. Schoenfeld, and P.M. Patroff,, *Nature* **405**, 926 (2000).

[6] D. Reuter, P. Kailuweit, A.D. Wieck, U. Zeitler, O. Wibbelhoff, C. Meier, A. Lorke, and J.C. Maan, *Phys. Rev. Lett.* **94**, 026808 (2005).

[7] *International Technology Roadmap for Semiconductors*, http://public.itrs.net

[8] D. Bimberg, N.N. Ledentsov, and M. Grundmann, *Quantum Dot Heterostructures* (Wiley, 1999).

[9] C.M. Lieber, *MRS Bulletin* **28**, 486 (2003).

[10] G. Bastard, *Wave Mechanics Applied to Semiconductor Heterostructures* (Les Editions de Physique, Les Ulis Cesex, 1988)

[11] C. Yannouleas and U. Landman, *Phys. Rev. Lett.* **82**, 5325 (1999); F. Troiani, H. Hohenester, and E. Molinari, *Phys. Rev. B* **65**, 161301 (2002); G. Bester, J. Shumway, and A. Zunger, *Phys. Rev. Lett.* **93**, 047401 (2004).

[12] F. Remacle and R.D. Levine, *J. Phys. Chem. B* **105**, 2153 (2001).

[13] P.S. Demle, A.W. Ghosh, and S. Datta, *Phys. Rev. B* **64**, 201403 (2001); M. Di Ventra, S.T. Pantelides, and N. Lang, *Phys. Rev. Lett.* **84**, 979 (2000).

[14] T. Mokari, E. Rothenberg, I. Popov, R. Costi, and U. Banin, *Science* **304**, 1787 (2004).

[15] A. Ferretti, A. Calzolari, R. Di Felice, F. Manghi, M.J. Caldas, M. Buongiorno Nardelli, and E. Molinari, *Phys. Rev. Lett.* **94**, 116802 (2005).

[16] L.E. Brus, *J. Chem. Phys.* **79**, 5566 (1983).

[17] Al.L. Efros and M. Rosen, *Annual Review of Materials Science* **30**, 475 (2000).

[18] H. Jiang and J. Singh, *Appl. Phys. Lett.* **71**, 3239 (1997); H. Fu, L.W. Wang, and A. Zunger, *Phys. Rev. B* **57**, 9971 (1998).

[19] A. Zunger, *Phys. Stat. Sol. A* **190**, 467 (2002).

[20] F. Pederiva, C.J. Umrigar, and E. Lipparini, *Phys. Rev. B* **62**, 8120 (2000); J. Shumway, A. Franceschetti, and A. Zunger, *Phys. Rev. B* **63**, 155316 (2001).

[21] O. Stier, M. Grundmann, and D. Bimberg, *Phys. Rev. B* **59**, 5688 (1999).

[22] P. Hawrylak and M. Korkusinski, *Topics in Applied Physics* **90**, 25 (2003).

[23] C. Delerue, M. Lannoo, and G. Allan, *Phys. Stat. Sol.* B **227**, 115 (2001).

[24] L. W. Wang and A. Zunger, *J. Chem. Phys.* **100**, 2394 (1994).

[25] S. Lee, J. Kim, L. Jonsson, J.W. Wilkins, G.W. Bryant, and G. Klimeck, *Phys. Rev. B* **66**, 235307 (2002).

[26] A. Franceschetti, H. Fu, L.W. Wang, and A. Zunger, *Phys. Rev. B* **60**, 1819 (1999).

[27] M. Rohlfing and S.G. Louie, *Phys. Rev. Lett.* **80**, 3320 (1998).

[28] A.J. Williamson, J. Grossman, R.Q. Hoods, A. Puzder, and G. Galli, *Phys. Rev. Lett.* **89**, 196803 (2002).

[29] L.W. Wang, *Phys. Rev. Lett.* **88**, 256402 (2002).

[30] L.W. Wang and J. Li, *Phys. Rev. B* **69**, 153302 (2004).

[31] S.H. Wei and A. Zunger, *Appl. Phys. Lett.* **72**, 2011 (1998).

[32] X. Cartoixa and L.W. Wang, *Phys. Rev. Lett.* **94**, 236804 (2005).

[33] L. He, G. Bester, and A. Zunger, cond-mat/0503492.

Figure captions

FIG.1 (color) Schematic diagram of the energy levels and wave functions of (a) wide-wire and (b) narrow-wire nano dumbbells, where coupling between the dots and the wire is neglected. The black solid lines show the conduction-band and valence-band offsets of bulk CdTe and CdSe. The levels h_{D1} and h_{D2} are the VBM states of the two dots. The levels e_{D1}, e_{D2} and e_W are the CBM states of the dots an the wire, respectively. In the case of (a) a wide wire, the hole wave functions are localized on the dots, while the electron wave function is localized on the wire. In the opposite case of (b) a wide wire, both electron and hole wave functions are localized on the dots.

FIG.3 (color) Calculated single-particles energies and wave functions of the three nano-dumbbells considered in this work. For each wire size, we show the atomistic wave functions of the topmost valence state (ψ_{vbm}) and the first three conduction-band states (ψ_1, ψ_2, and ψ_3). Also shown are the single-particle energies (in meV), measured with respect to the CBM ($\varepsilon_1 = 0$).

FIG. 4 (color) Schematic diagram of the single-particle levels of the isolated building blocks (wire and dots) and of the coupled (wire+dots) system. Wire states are shown in blue, dot states in red.

FIG.5 (color) Energy levels (in meV) of two electrons in a wide-wire nano dumbbell (R_W = 15 Å). The correlation function in the uncorrelated (single-particle) and correlated (full CI) cases is shown at the bottom of the figure. The correlation function gives the

probability of finding one electron in different regions of the dumbbells (yellow cloud), when the other electron is kept fixed at the position of the blue circle.

FIG.6 (color) Energy levels (in meV) of two electrons in a narrow-wire nano dumbbell (R_W = 8 Å). The correlation function in the uncorrelated (single-particle) and correlated (full CI) cases is shown at the bottom of the figure. The correlation function gives the probability of finding one electron in different regions of the dumbbells (yellow cloud), when the other electron is kept fixed at the position of the blue circle.

FIG.7 (color) Energy levels (in meV) of two electrons in an intermediate-wire nano dumbbell (R_W = 10 Å). The correlation function in the uncorrelated (single-particle) and correlated (full CI) cases is shown at the bottom of the figure. The correlation function gives the probability of finding one electron in different regions of the dumbbells (yellow cloud), when the other electron is kept fixed at the position of the blue circle.

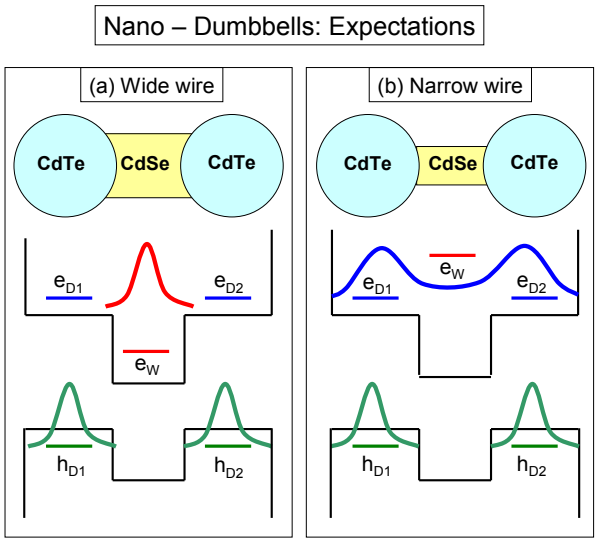
Nano – Dumbbells: Expectations
(a) Wide wire
CdTe
CdSe
CdTe
e_{D1}
e_{D2}
e_W
h_{D1}
h_{D2}
(b) Narrow wire
CdTe
CdSe
CdTe
e_{D1}
e_W
e_{D2}
h_{D1}
h_{D2}

Fig. 1

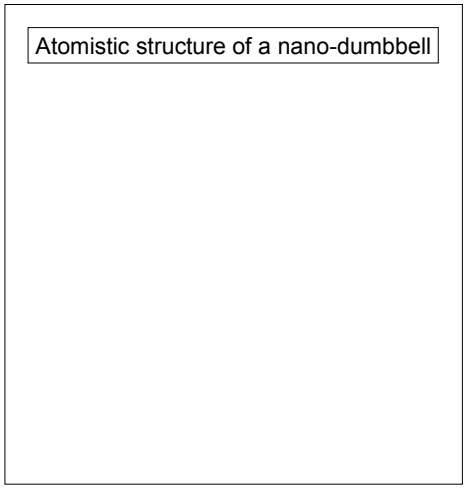
Atomistic structure of a nano-dumbbell

Fig. 2

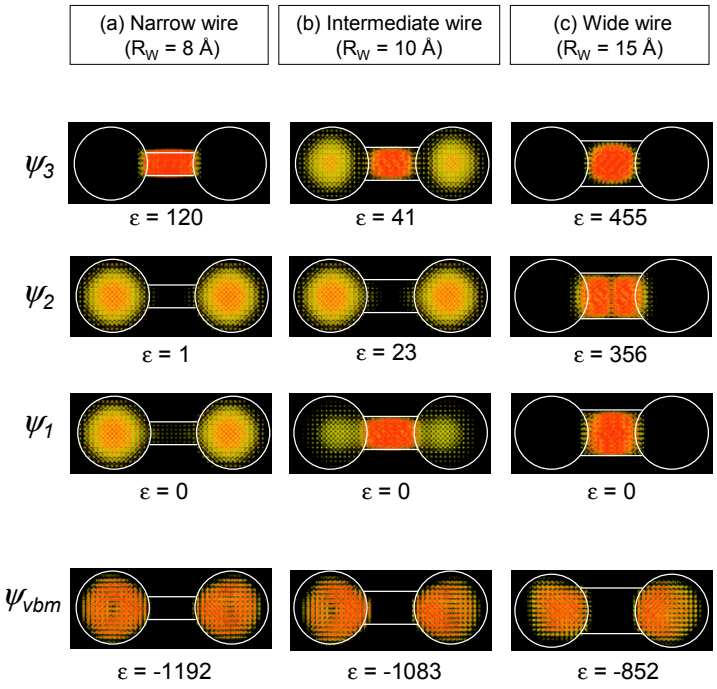
(a) Narrow wire
(R_W = 8 Å)
(b) Intermediate wire
(R_W = 10 Å)
(c) Wide wire
(R_W = 15 Å)
ψ_3
ε = 120
ε = 41
ε = 455
ψ_2
ε = 1
ε = 23
ε = 356
ψ_1
ε = 0
ε = 0
ε = 0
ψ_{vbm}
ε = -1192
ε = -1083
ε = -852

Fig. 3

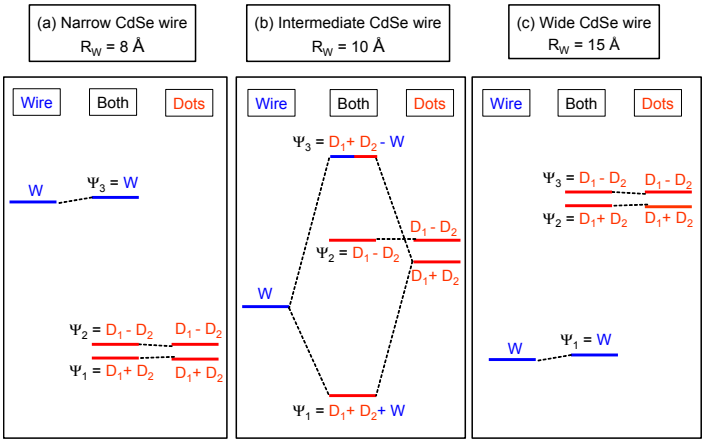
(a) Narrow CdSe wire
R_W = 8 Å
Wire
Both
Dots
W
Ψ_3 = W
Ψ_2 = D_1 - D_2
D_1 - D_2
Ψ_1 = D_1+ D_2
D_1+ D_2
(b) Intermediate CdSe wire
R_W = 10 Å
Wire
Both
Dots
Ψ_3 = D_1+ D_2 - W
D_1 - D_2
Ψ_2 = D_1 - D_2
W
D_1+ D_2
Ψ_1 = D_1+ D_2+ W
(c) Wide CdSe wire
R_W = 15 Å
Wire
Both
Dots
Ψ_3 = D_1 - D_2
D_1 - D_2
Ψ_2 = D_1+ D_2
D_1+ D_2
W
Ψ_1 = W

Fig. 4

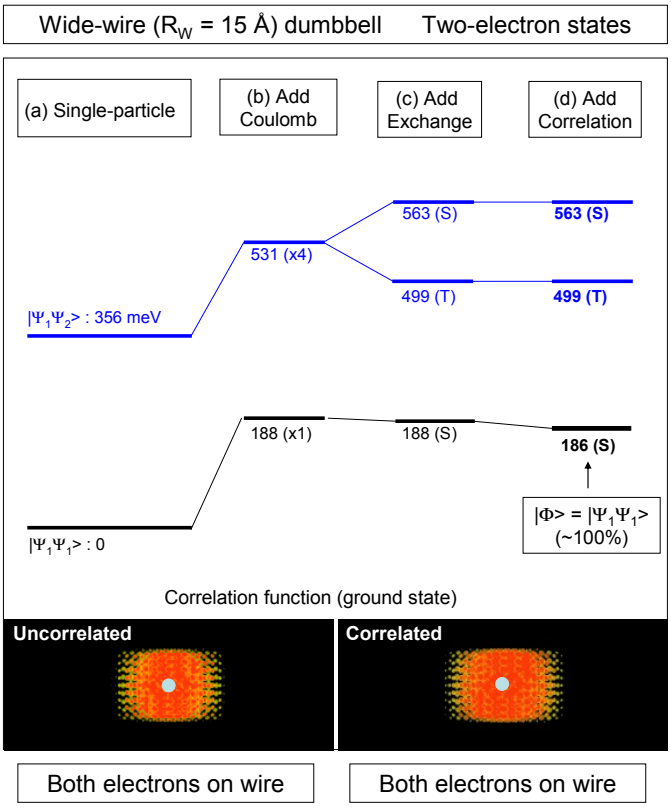
Wide-wire (R_W = 15 Å) dumbbell Two-electron states
(a) Single-particle
(b) Add Coulomb
(c) Add Exchange
(d) Add Correlation
563 (S)
563 (S)
531 (x4)
499 (T)
499 (T)
$|\Psi_1\Psi_2\rangle$: 356 meV
188 (x1)
188 (S)
186 (S)
$|\Phi\rangle = |\Psi_1\Psi_1\rangle$ (~100%)
$|\Psi_1\Psi_1\rangle$: 0
Correlation function (ground state)
Uncorrelated
Correlated
Both electrons on wire
Both electrons on wire

Fig. 5

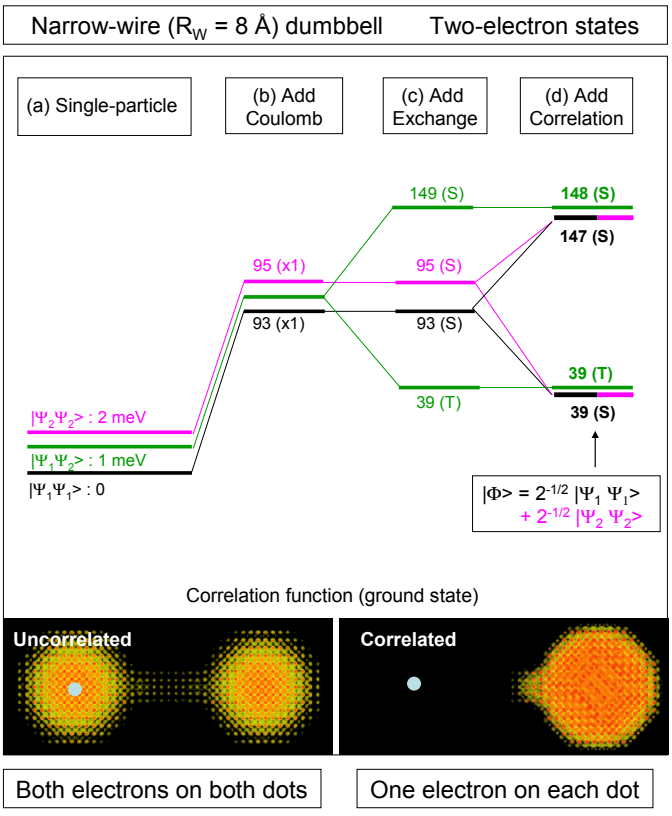
Narrow-wire (R_W = 8 Å) dumbbell
Two-electron states
(a) Single-particle
(b) Add Coulomb
(c) Add Exchange
(d) Add Correlation
149 (S)
148 (S)
147 (S)
95 (x1)
95 (S)
93 (x1)
93 (S)
39 (T)
39 (T)
39 (S)
$|\Psi_2\Psi_2\rangle$: 2 meV
$|\Psi_1\Psi_2\rangle$: 1 meV
$|\Psi_1\Psi_1\rangle$: 0
$|\Phi\rangle = 2^{-1/2} |\Psi_1 \Psi_1\rangle + 2^{-1/2} |\Psi_2 \Psi_2\rangle$
Correlation function (ground state)
Uncorrelated
Correlated
Both electrons on both dots
One electron on each dot

Fig. 6

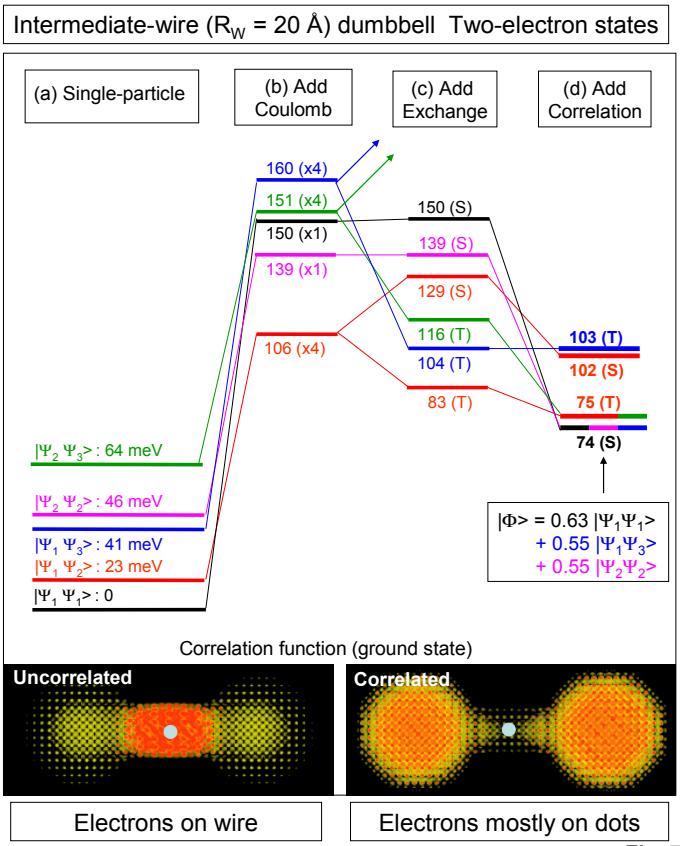
Intermediate-wire (R_W = 20 Å) dumbbell Two-electron states
(a) Single-particle
(b) Add Coulomb
(c) Add Exchange
(d) Add Correlation
160 (x4)
151 (x4)
150 (x1)
139 (x1)
106 (x4)
150 (S)
139 (S)
129 (S)
116 (T)
104 (T)
83 (T)
103 (T)
102 (S)
75 (T)
74 (S)
$|\Psi_2\Psi_3\rangle$: 64 meV
$|\Psi_2\Psi_2\rangle$: 46 meV
$|\Psi_1\Psi_3\rangle$: 41 meV
$|\Psi_1\Psi_2\rangle$: 23 meV
$|\Psi_1\Psi_1\rangle$: 0
$|\Phi\rangle$ = 0.63 $|\Psi_1\Psi_1\rangle$
+ 0.55 $|\Psi_1\Psi_3\rangle$
+ 0.55 $|\Psi_2\Psi_2\rangle$
Correlation function (ground state)
Uncorrelated
Correlated
Electrons on wire
Electrons mostly on dots

Fig. 7